Supporting Information

Electrocatalytic Properties of Binuclear Cu(II) Fused Porphyrins for Hydrogen Evolution

Khusnutdinova, D.[†]; Wadsworth, B. L.[†]; Flores, M.; Beiler, A. M.; Reyes Cruz, E. A.; Zenkov, Y.; and Moore, G. F.*
School of Molecular Sciences and the Biodesign Institute Center for Applied Structural Discovery (CASD)
Arizona State University, Tempe, AZ 85287-1604, United States
gfmoore@asu.edu

Index

1. **Additional Information on Experimental Methods** **S2**
2. **NMR Data** **S4**
3. **Optical Characterization** **S6**
4. **FTIR Data** **S8**
5. **XPS Data** **S9**
6. **UV–vis-NIR-SEC and IR-SEC Data** **S10**
7. **Electrochemical Data** **S12**
8. **Rotating Ring-Disk Experiments** **S26**
9. **Acid Stability** **S30**
10. **The HA/H_2 Equilibrium Potential in Dichloromethane** **S32**
11. **Supporting Information References** **S33**

1. Additional Information on Experimental Methods

Synthesis

Copper(II) 5,10,15,20-tetra-*p*-tolylporphyrin (**CuP**) was prepared following a modified version of previously reported procedures.[1-3] A mixture containing 5,10,15,20-tetra-*p*-tolylporphyrin (50 mg, 0.075 mmol) and copper(II) acetate (95 mg, 0.53 mmol) in a solution of chloroform (35 mL) and methanol (5 mL) was stirred at reflux for 15 hours. Upon cooling, the mixture was washed with a saturated solution of aqueous sodium bicarbonate, then with a saturated solution of aqueous sodium chloride, before extracting with dichloromethane. The organic phase was dried over sodium sulfate, filtered, and the solvent evaporated at reduced pressure. The residue was purified by column chromatography on alumina using dichloromethane as the eluent. Recrystallization from dichloromethane/methanol gave the target compound (96%). Fourier transform infrared (FTIR), electron paramagnetic resonance (EPR), and UV–vis absorption spectroscopies coupled with mass spectrometry confirm successful synthesis of the target compounds and the data obtained using these methods are in agreement with previous reports.[1-3]

Bicopper(II) *meso*-β doubly-fused 5,24-di(*p*-tolyl)-10,19,29,38-tetramesitylporphyrin (**Cu_2FP**) and *meso*-β doubly-fused 5,24-di(*p*-tolyl)-10,19,29,38-tetramesitylporphyrin were prepared using previously reported methods.[4] Nuclear magnetic resonance (NMR) and UV–vis absorption spectroscopies coupled with mass spectrometry confirm successful synthesis of the target compounds and the data obtained using these methods are in agreement with previous reports. Additional characterization of **Cu_2FP** was performed using Fourier transform infrared (FTIR) and electron paramagnetic resonance (EPR) spectroscopies. FTIR (KBr): 1610, 1506, 1450, 1379, 1358, 1327, 1230, 1209, 1182, 1161, 1065, 1003 cm^{-1}.
EPR (g_x= 2.021).

NMR

^{1}H Nuclear magnetic resonance (NMR) spectra were recorded on a Varian NMR spectrometer operating at 400 MHz. Unless otherwise stated, all spectra were collected at room temperature.

EPR

Spin Hamiltonian. The EPR spectrum of the monomeric copper(II) porphyrin was analyzed considering a single Cu(II) ion (S = 1/2). Thus, the EPR data was fit using a spin Hamiltonian, *H*, containing the electron Zeeman interaction with the applied magnetic field $\boldsymbol{B_0}$, and the hyperfine coupling (hfc) interactions with one ^{63}Cu (I = 3/2), four equivalent ^{14}N (I = 1) and one ^{1}H (I = 1/2):[5]

$$H = \boldsymbol{\beta_e S . g . B_0} + h\,\boldsymbol{S . A^{Cu_i} . I^{Cu_i}} + \sum_{j=1}^{4} h\,\boldsymbol{S . A^{N_j} . I^{N_j}} + h\,\boldsymbol{S . A^{H} . I^{H}} \qquad Eq\ (1)$$

where $\boldsymbol{S}$ is the electron spin operator, $\boldsymbol{I^{Cu_i}}$, $\boldsymbol{I^{N_j}}$ and $\boldsymbol{I^{H}}$ are the nuclear spin operators of a ^{63}Cu, four equivalent ^{14}N and a ^{1}H, respectively, $\boldsymbol{A^{Cu_i}}$, $\boldsymbol{A^{N_j}}$ and $\boldsymbol{A^{H}}$ are the corresponding hfc tensors in frequency units, $\boldsymbol{g}$ is the electronic *g*-tensor, $\boldsymbol{\beta_e}$ is the electron magneton, and *h* is Planck's constant.
The EPR spectrum of the fused copper(II) porphyrins was analyzed considering two equivalent Cu(II) ions (S = 1/2) interacting with two equivalent ^{63}Cu nuclei. In this case, only the electron Zeeman term and the hfc interactions with two equivalent ^{63}Cu (I = 3/2) nuclei were included in the spin Hamiltonian since hfc interactions with ^{14}N and ^{1}H are not resolved in the spectrum.

Fitting of EPR spectra. To quantitatively compare experimental and simulated spectra, we divided the spectra into *N* intervals, *i.e.*, we treated the spectrum as an *N*-dimensional vector $\boldsymbol{R}$. Each component R_j has the amplitude of the EPR signal at a magnetic field B_j, with *j* varying from 1 to *N*. The amplitudes of the experimental and simulated spectra were normalized so that the span between the maximum and minimum values of R_j is 1. We compared the calculated amplitudes R_j^{calc} of the signal with the observed values R_j defining a root-mean-square deviation σ by:

$$\sigma(p_1, p_2, \ldots, p_n) = [\sum_j (R_j^{calc}(p_1, p_2, \ldots, p_n) - R_j^{exp})^2/N]^{1/2} \qquad Eq\ (2)$$

where the sums are over the N values of j, and p's are the fitting parameters that produced the calculated spectrum. For our simulations, N was set equal to 2048. The EPR spectra were simulated using EasySpin (version 5.2.11), a computational package developed by Stoll and Schweiger[6] and based on Matlab (The MathWorks, Massachusetts, USA). EasySpin calculates EPR resonance fields using the energies of the states of the spin system obtained by direct diagonalization of the spin Hamiltonian (*Eq 1*). The EPR fitting procedure used a Monte Carlo type iteration to minimize the root-mean-square deviation, σ (*Eq 2*), between measured and simulated spectra. We searched for the optimum values of the following parameters: the principal components of $\boldsymbol{g}$ (g_x, g_y, and g_z), the principal components of the hfc tensors $\boldsymbol{A}^{Cu_i}$ ($A_x^{Cu_i}$, $A_y^{Cu_i}$, $A_z^{Cu_i}$), $\boldsymbol{A}^{N_j}$ ($A_x^{N_j}$, $A_y^{N_j}$, $A_z^{N_j}$) and $\boldsymbol{A}^{H}$ (A_x^{H}, A_y^{H}, A_z^{H}), and the peak-to-peak line widths (ΔB_x, ΔB_y and ΔB_z).

2. NMR Data

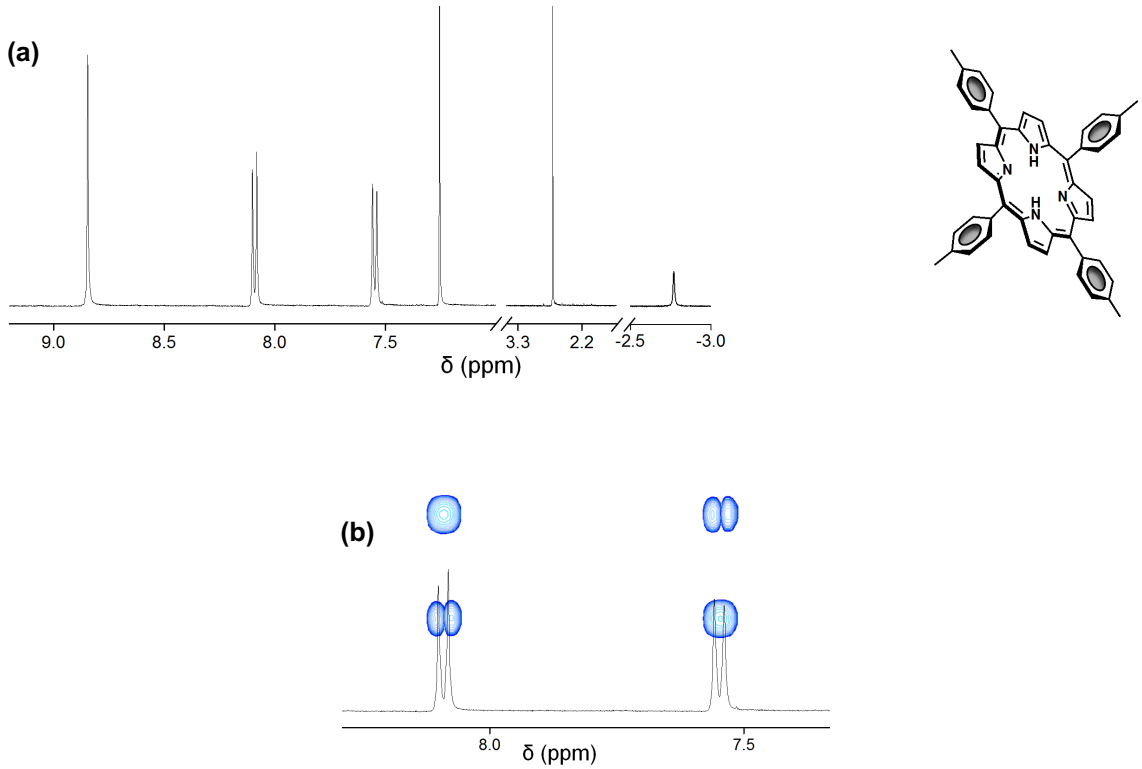

Figure S1. (a) ^{1}H NMR spectrum (black line) and (b) ^{1}H NMR spectrum (black line) with overlaid COSY (blue lines) of 5,10,15,20-tetra-*p*-tolylporphyrin in chloroform-d.

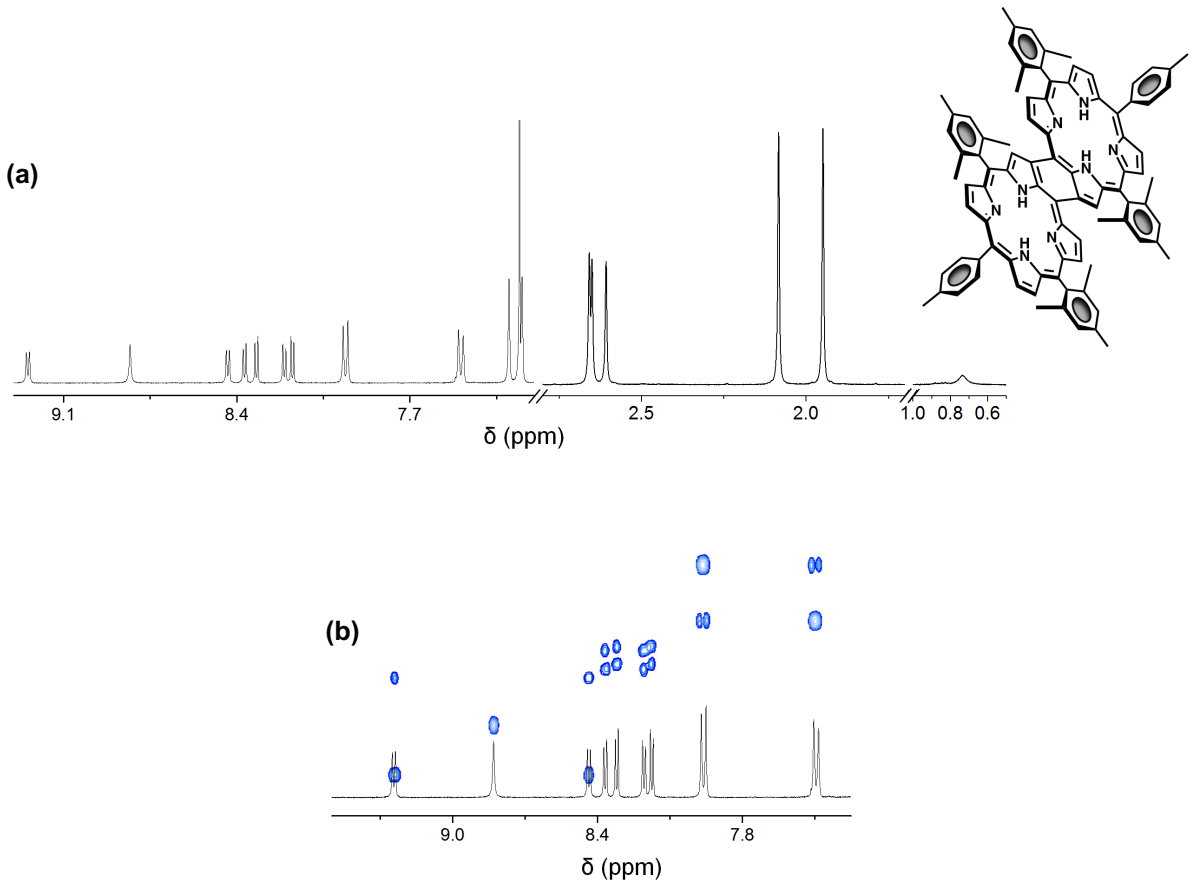

Figure S2. (a) ^{1}H NMR spectrum (black line) and (b) ^{1}H NMR spectrum (black line) with overlaid COSY (blue lines) of *meso*-β doubly-fused 5,24-di(*p*-tolyl)-10,19,29,38-tetramesitylporphyrin in chloroform-d.

3. Optical Characterization

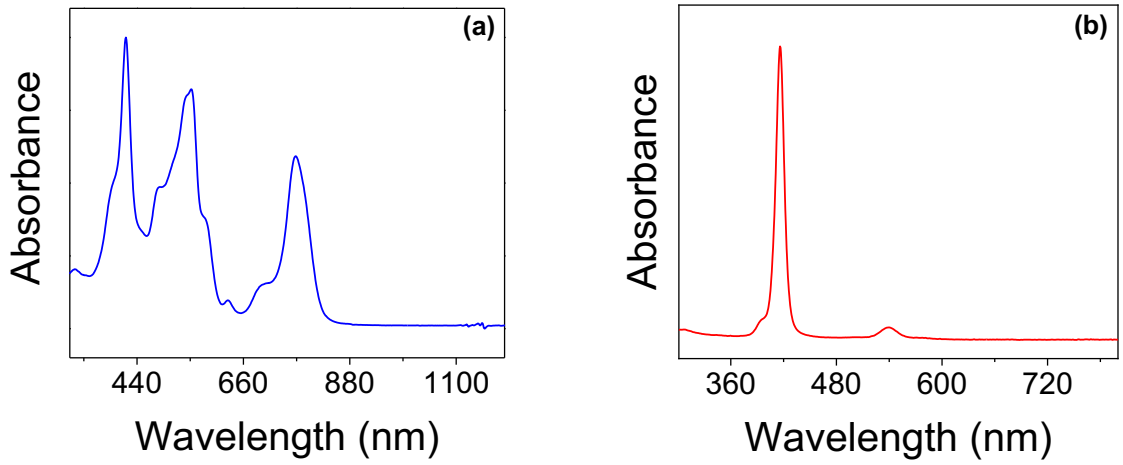

Figure S3. Absorption spectra of (a) **Cu_2FP** and (b) **CuP** recorded in dichloromethane.

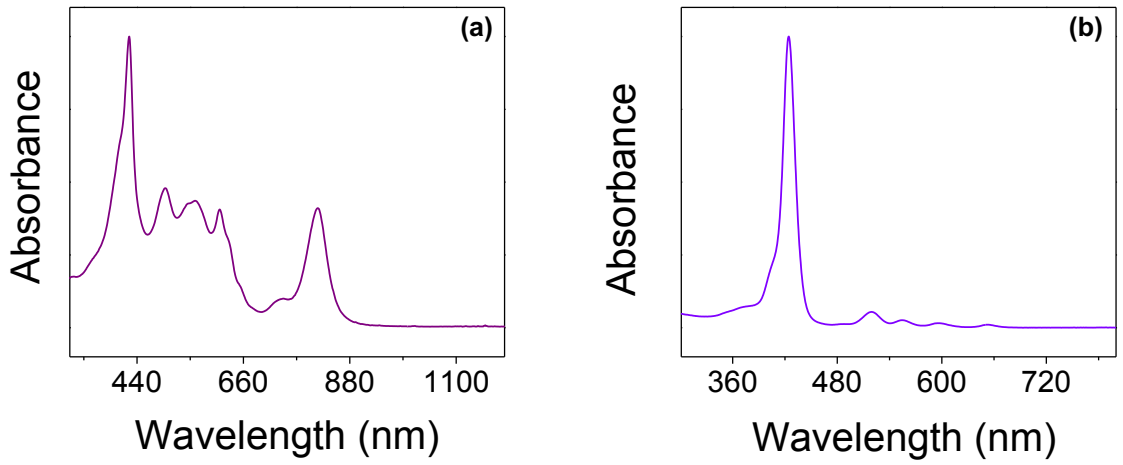

Figure S4. Absorption spectra of (a) *meso*-β doubly-fused 5,24-di(*p*-tolyl)-10,19,29,38-tetramesitylporphyrin and (b) 5,10,15,20-tetra-*p*-tolylporphyrin recorded in dichloromethane.

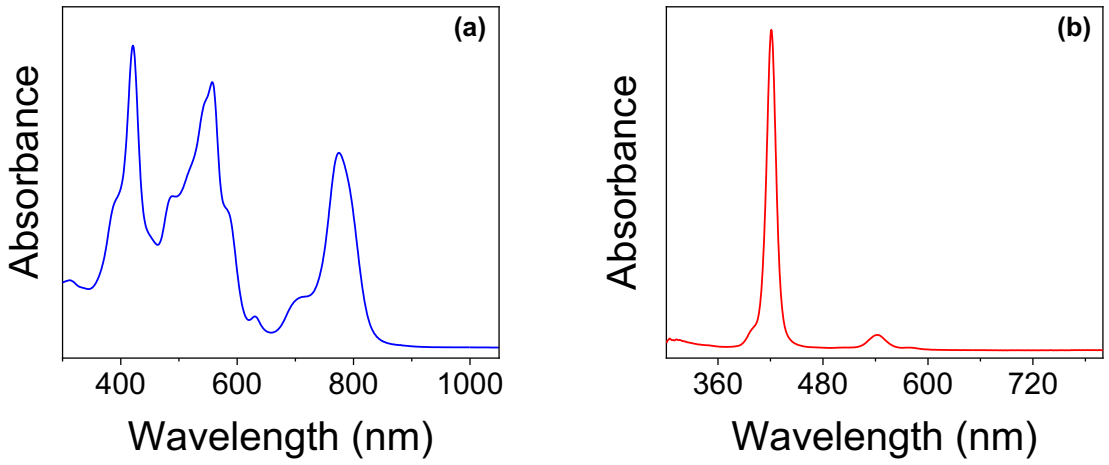

Figure S5. Absorption spectra of (a) **Cu_2FP** and (b) **CuP** recorded in benzonitrile.

4. FTIR Data

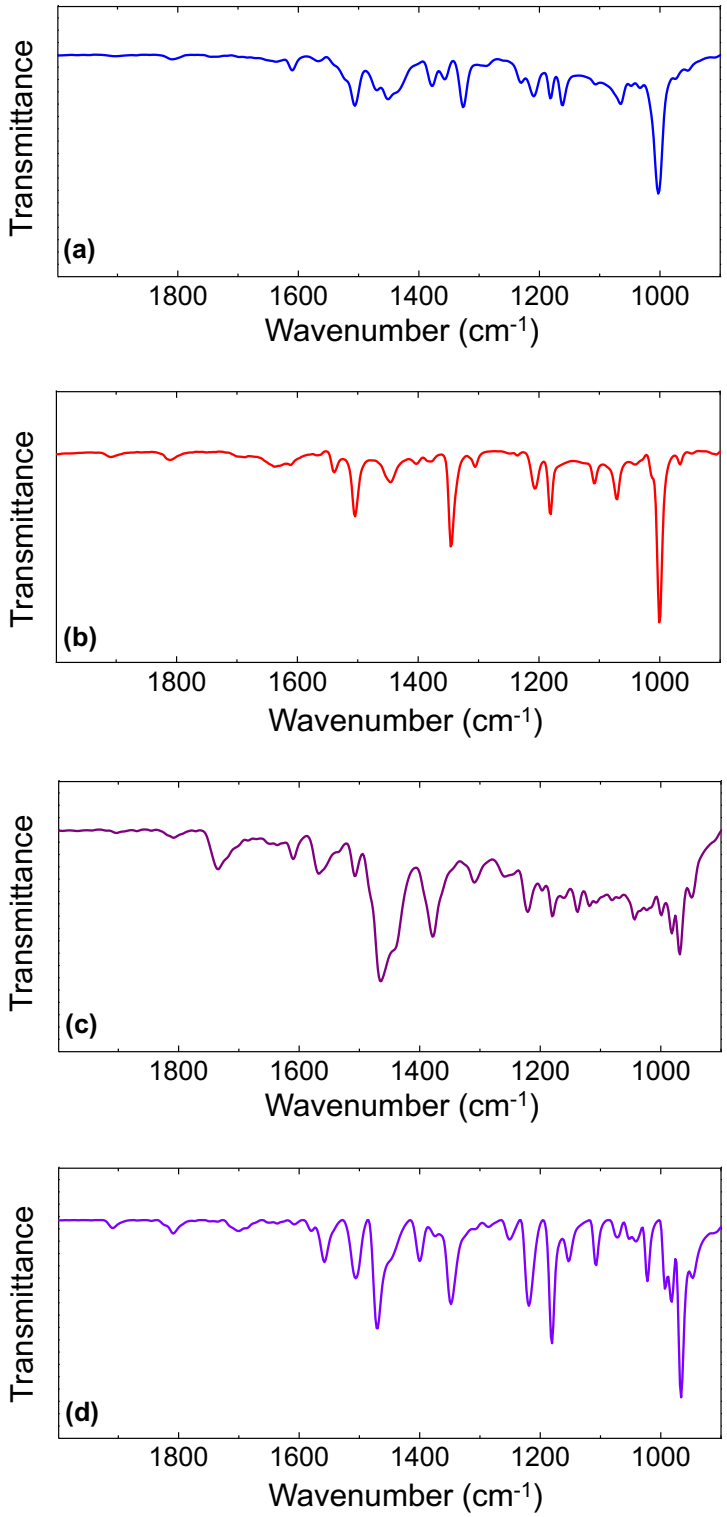

Figure S6. FTIR transmission spectra of (a) **Cu_2FP**, (b) **CuP**, (c) *meso*-β doubly-fused 5,24-di(*p*-tolyl)-10,19,29,38-tetramesitylporphyrin, and (d) 5,10,15,20-tetra-*p*-tolylporphyrin in KBr.

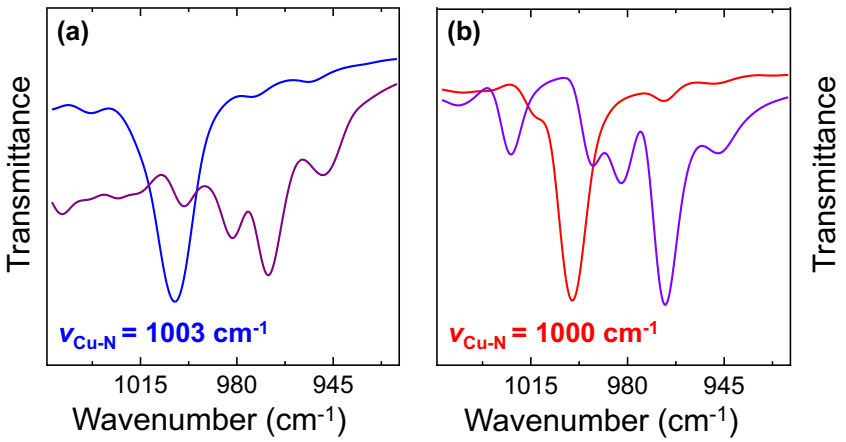

Figure S7. FTIR transmission spectra of (a) **Cu_2FP** (blue) and *meso*-β doubly-fused 5,24-di(*p*-tolyl)-10,19,29,38-tetramesitylporphyrin (purple) as well as (b) **CuP** (red) and 5,10,15,20-tetra-*p*-tolylporphyrin (violet) showing the frequency region associated with the in-plane porphyrin deformation mode labeled as ν_{Cu-N} (where ν is the vibrational frequency).

5. XP Spectroscopy Data

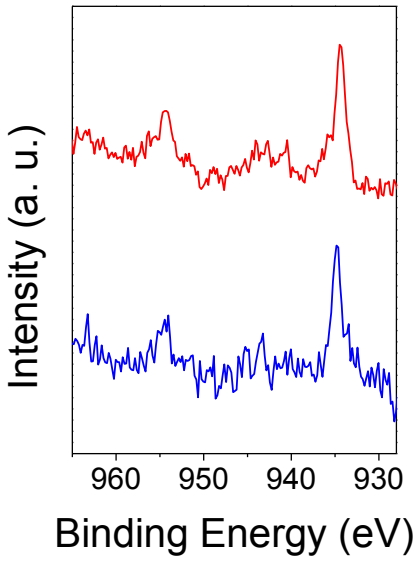

Figure S8. High-energy resolution core level XP spectra of the Cu 2p region recorded using samples of **Cu_2FP** (blue) or **CuP** (red) dropcast onto a glassy carbon disk.

6. UV–vis-NIR-SEC and IR-SEC Data

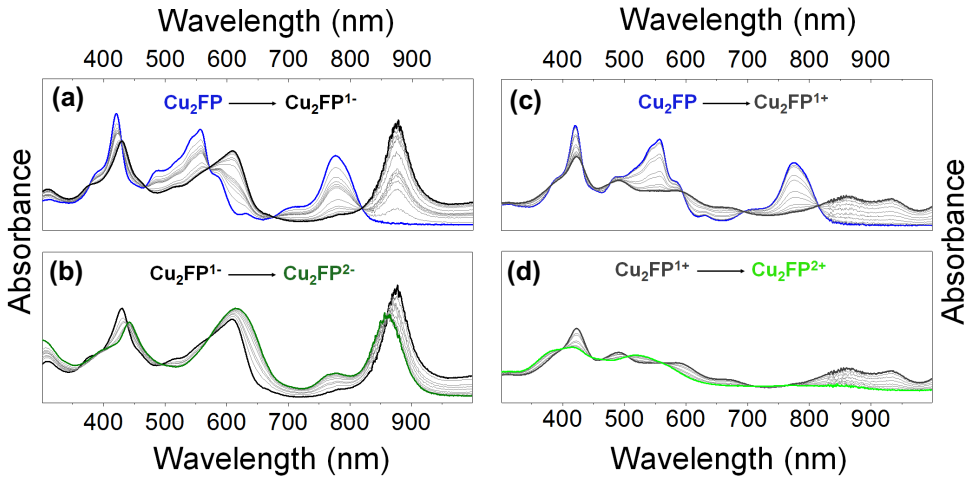

Figure S9. UV–vis-NIR absorption spectra of **Cu_2FP** (6.5 μM) recorded in a 0.1 M tetrabutylammonium hexafluorophosphate ($TBAPF_6$) benzonitrile solution polarized at potentials to generate (a and b) **Cu_2FP** (blue), **Cu_2FP^{1-}** (black), and **Cu_2FP^{2-}** (green) as well as (c and d) **Cu_2FP** (blue), **Cu_2FP^{1+}** (gray), and **Cu_2FP^{2+}** (light green).

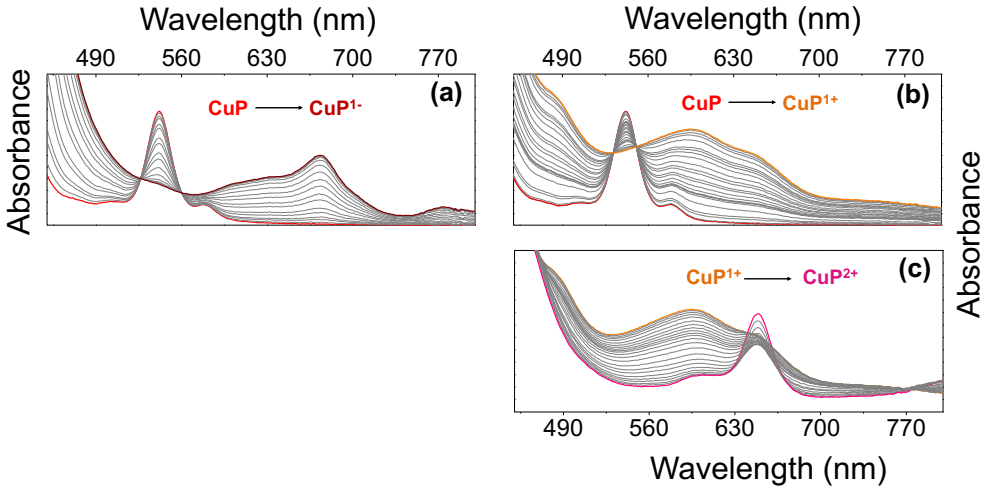

Figure S10. UV–vis absorption spectra of **CuP** (25 μM) recorded in a 0.1 M $TBAPF_6$ benzonitrile solution polarized at potentials to generate (a) **CuP** (red) and **CuP^{1-}** (dark red), as well as (b and c) **CuP** (red), **CuP^{1+}** (orange), and **CuP^{2+}** (pink).

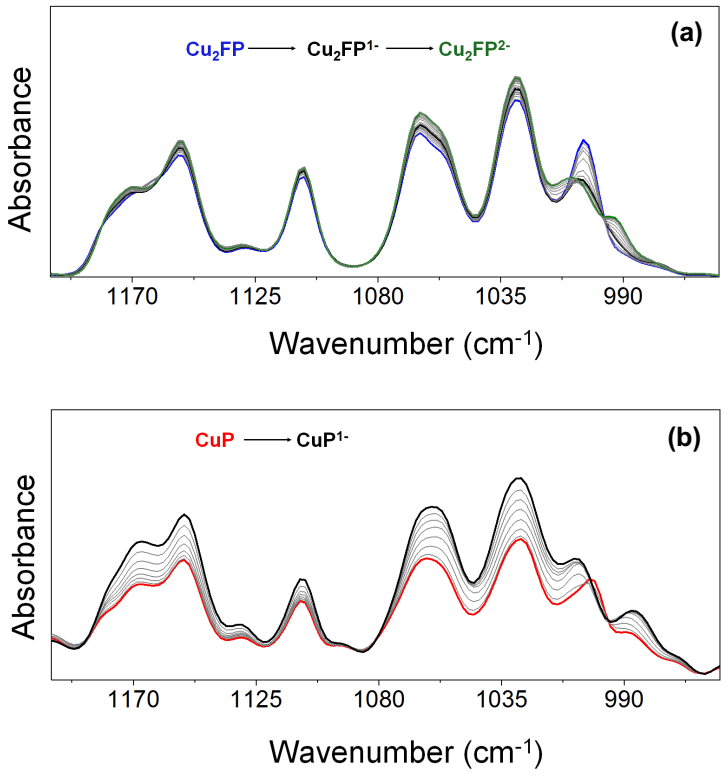

Figure S11. FTIR absorption spectra of (a) **Cu_2FP** (0.4 mM) polarized at potentials to generate **Cu_2FP** (blue), **Cu_2FP^{1-}** (black), and **Cu_2FP^{2-}** (green) as well as (b) **CuP** (0.4 mM) polarized at potentials to generate **CuP** (red) and **CuP^{1-}** (black). All spectra were collected in a 0.1 M $TBAPF_6$ dichloromethane solution.

7. Electrochemical Data

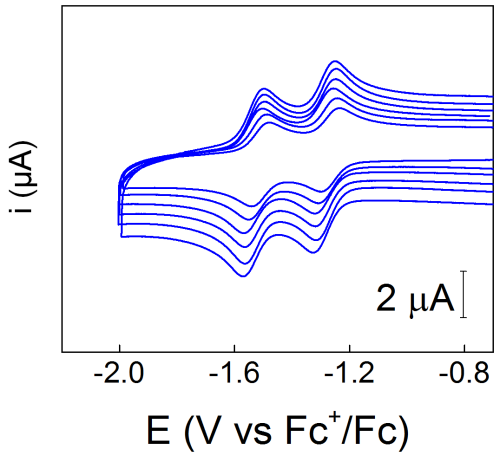

Figure S12. Cyclic voltammograms of **Cu_2FP** (0.34 mM) recorded in a 0.1 M $TBAPF_6$ dichloromethane solution under argon at scan rates of 50–500 mV s^{-1}. All voltammograms were recorded using a 3 mm diameter glassy carbon working electrode at room temperature and the ferrocenium/ferrocene redox couple as an internal reference.

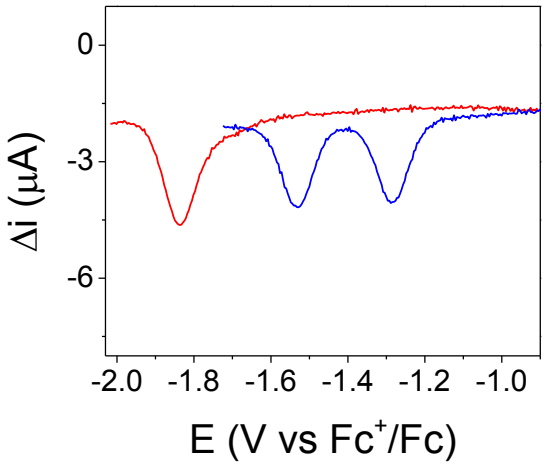

Figure S13. Differential pulse voltammetry data recorded using **Cu_2FP** (0.1 mM) (blue) or **CuP** (0.1 mM) (red) in a 0.1 M $TBAPF_6$ dichloromethane solution under argon. All measurements were recorded using a 3 mm diameter glassy carbon working electrode at room temperature and the ferrocenium/ferrocene redox couple as an internal reference.

Table S1. Midpoint potentials for the reduction and oxidation ($^{n}E_{1/2}$) of **Cu_2FP** or **CuP** complexes as determined by cyclic voltammetry. Peak–to–peak separations (ΔE_p) are reported in parentheses. All voltammograms were collected in a 0.1 M $TBAPF_6$ ***benzonitrile*** solution under argon using a 3 mm diameter glassy carbon working electrode at room temperature and the ferrocenium/ferrocene redox couple as an internal reference.

Compound	^{n}E (V vs Fc^+/Fc)			
	^{II}E (ΔE_p, mV)	^{I}E (ΔE_p, mV)	^{i}E (ΔE_p, mV)	^{ii}E (ΔE_p, mV)
Cu_2FP	-1.52 (69)	-1.23 (65)	+0.34 (65)	0.56 (70)
CuP	N/A	-1.80 (82)	+0.47 (94)	0.87 (99)

Table S2. Midpoint potentials for the reduction and oxidation ($^{n}E_{1/2}$) of **Cu_2FP** or **CuP** complexes as determined by cyclic voltammetry. Peak–to–peak separations (ΔE_p) are reported in parentheses. All voltammograms were collected in a 0.1 M $TBAPF_6$ ***dichloromethane*** solution under argon using a 3 mm diameter glassy carbon working electrode at room temperature and the ferrocenium/ferrocene redox couple as an internal reference.

Compound	^{n}E (V vs Fc^+/Fc)			
	^{II}E (ΔE_p, mV)	^{I}E (ΔE_p, mV)	^{i}E (ΔE_p, mV)	^{ii}E (ΔE_p, mV)
Cu_2FP	-1.53 (105)	-1.27 (102)	+0.27(69)	0.56(77)
CuP	N/A	-1.84 (92)	+0.44 (90)	0.85(96)

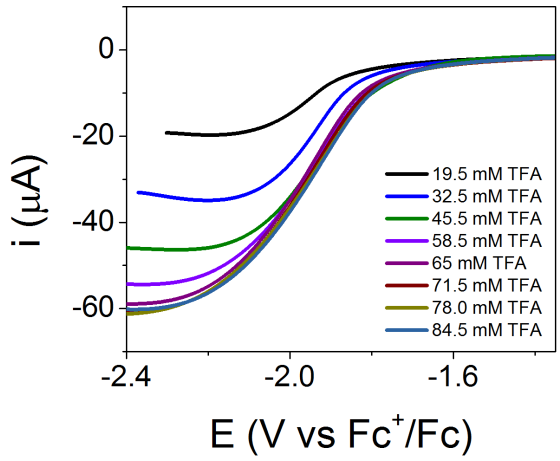

Figure S14. Voltammograms of **Cu_2FP** (0.01 mM) collected in a 0.1 M $TBAPF_6$ dichloromethane solution under argon with an increasing amount of TFA (19.5–84.5 mM) and at a scan rate of 600 mV s^{-1}. All voltammograms were recorded using a 1 mm diameter glassy carbon working electrode at room temperature and the ferrocenium/ferrocene redox couple as an internal reference. The return scans were excluded for clarity.

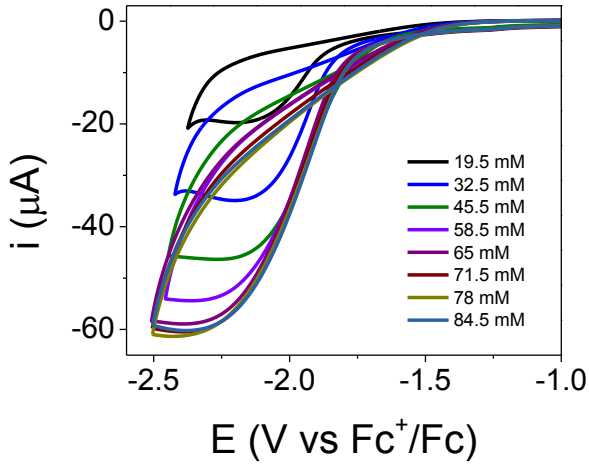

Figure S15. Cyclic voltammograms of **Cu_2FP** (0.01 mM) collected in a 0.1 M $TBAPF_6$ dichloromethane solution under argon with an increasing amount of TFA (19.5–84.5 mM) and at a scan rate of 600 mV s^{-1}. All voltammograms were recorded using a 1 mm diameter glassy carbon working electrode at room temperature and the ferrocenium/ferrocene redox couple as an internal reference.

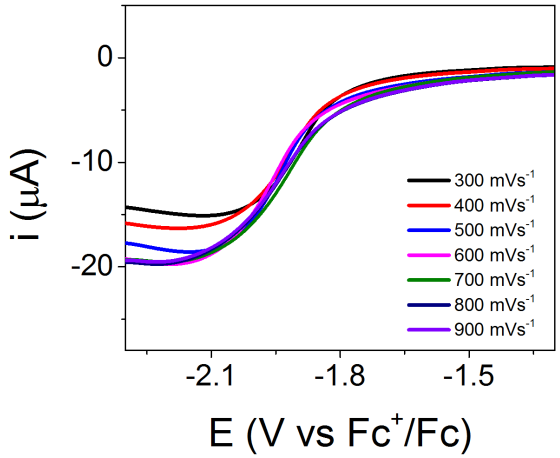

Figure S16. Voltammograms of **Cu_2FP** (0.01 mM) collected in a 0.1 M $TBAPF_6$ dichloromethane solution under argon with TFA (19.5 mM) and at scan rates of 300 (black), 400 (red), 500 (blue), 600 (pink), 700 (green), 800 (navy), and 900 (purple) mV s^{-1}. All voltammograms were recorded using a 1 mm diameter glassy carbon working electrode at room temperature and the ferrocenium/ferrocene redox couple as an internal reference. The return scans were excluded for clarity.

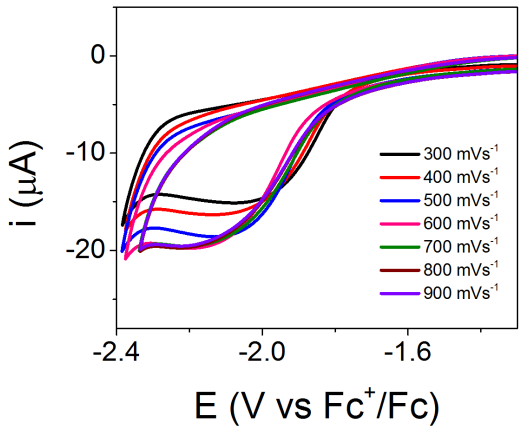

Figure S17. Cyclic voltammograms of **Cu_2FP** (0.01 mM) collected in a 0.1 M $TBAPF_6$ dichloromethane solution under argon with TFA (19.5 mM) and at scan rates of 300 (black), 400 (red), 500 (blue), 600 (pink), 700 (green), 800 (navy), and 900 (purple) mV s^{-1}. All voltammograms were recorded using a 1 mm diameter glassy carbon working electrode at room temperature and the ferrocenium/ferrocene redox couple as an internal reference.

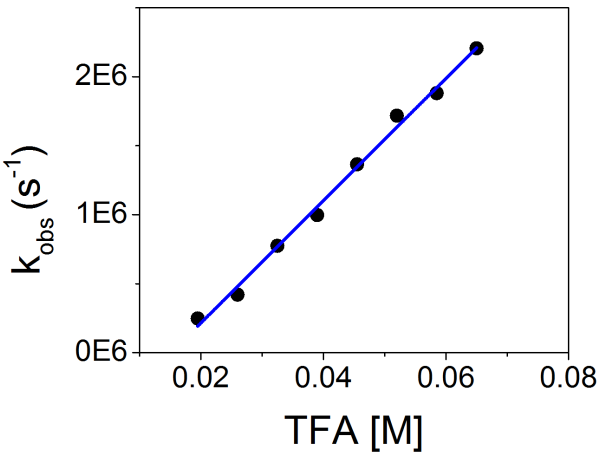

Figure S18. Plot of k_{obs} versus the concentration of TFA. The data points used to calculate k_{obs} are the i_{cat}/i_p values from the plot of i_{cat}/i_p versus the square root of the concentration of TFA shown in Figure 4c of the main text. The last two data points, in which k_{obs} is independent of the acid concentration are omitted. R^2 = 0.993. Slope = 4.43 x 10^7.

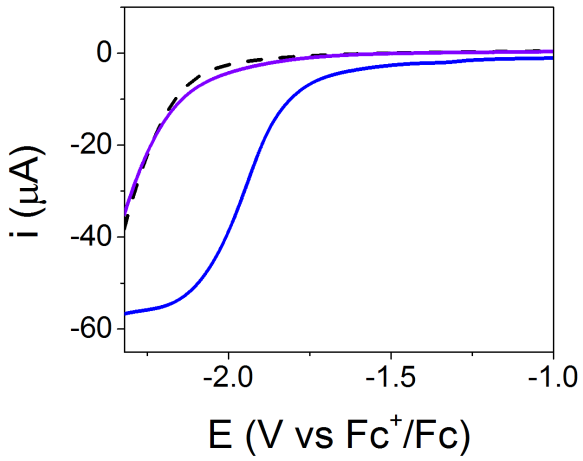

Figure S19. Linear sweep voltammograms recorded using a glassy carbon working electrode in a 0.01 mM **Cu_2FP** solution (blue solid) or in a solution without **Cu_2FP** present, following collection of the blue linear sweep voltammogram and rinsing the electrode surface with fresh dichloromethane (purple solid). A voltammogram of a freshly polished glassy carbon electrode is included for comparison (black dash). All voltammograms were recorded at a scan rate of 100 mV s^{-1} in a 0.1 M $TBAPF_6$ dichloromethane solution with 65 mM TFA using a 1 mm diameter working electrode and the ferrocenium/ferrocene redox couple as an internal reference.

Table S3. Experimental results from an acid titration of **Cu_2FP** (0.01 mM). These results were used to construct Figure 4c in the main text and Figure S18 in the supplemental information file.

[TFA] (M)	i_{cat} (μA)	i_p (μA)	i_{cat}/i_p	k_{obs} (s^{-1})
2.0×10^{-2}	2.0×10^{1}	4.3×10^{-2}	0.5×10^{3}	0.2×10^{6}
2.6×10^{-2}	2.6×10^{1}	4.3×10^{-2}	0.6×10^{3}	0.4×10^{6}
3.3×10^{-2}	3.5×10^{1}	4.3×10^{-2}	0.8×10^{3}	0.8×10^{6}
3.9×10^{-2}	4.0×10^{1}	4.3×10^{-2}	0.9×10^{3}	1.0×10^{6}
4.6×10^{-2}	4.6×10^{1}	4.3×10^{-2}	1.1×10^{3}	1.4×10^{6}
5.2×10^{-2}	5.2×10^{1}	4.3×10^{-2}	1.2×10^{3}	1.7×10^{6}
5.9×10^{-2}	5.4×10^{1}	4.3×10^{-2}	1.3×10^{3}	1.9×10^{6}
6.5×10^{-2}	5.9×10^{1}	4.3×10^{-2}	1.4×10^{3}	2.2×10^{6}
7.2×10^{-2}	6.0×10^{1}	4.3×10^{-2}	1.4×10^{3}	2.3×10^{6}
7.8×10^{-2}	6.1×10^{1}	4.3×10^{-2}	1.4×10^{3}	2.4×10^{6}
8.5×10^{-2}	6.0×10^{1}	4.3×10^{-2}	1.4×10^{3}	2.3×10^{6}

Table S4. Experimental results from an acid titration of **Cu_2FP** (0.01 mM).

[TFA] (M)	i_{cat} (μA)	i_p (μA)	i_{cat}/i_p	k_{obs} (s^{-1})
2.0×10^{-2}	1.7×10^{1}	4.2×10^{-2}	0.4×10^{3}	0.2×10^{6}
2.6×10^{-2}	2.2×10^{1}	4.2×10^{-2}	0.5×10^{3}	0.3×10^{6}
3.3×10^{-2}	3.1×10^{1}	4.2×10^{-2}	0.7×10^{3}	0.6×10^{6}
3.9×10^{-2}	3.6×10^{1}	4.2×10^{-2}	0.9×10^{3}	0.8×10^{6}
4.6×10^{-2}	4.3×10^{1}	4.2×10^{-2}	1.0×10^{3}	1.2×10^{6}
5.2×10^{-2}	5.0×10^{1}	4.2×10^{-2}	1.2×10^{3}	1.6×10^{6}
5.9×10^{-2}	5.2×10^{1}	4.2×10^{-2}	1.2×10^{3}	1.7×10^{6}
6.5×10^{-2}	5.8×10^{1}	4.2×10^{-2}	1.4×10^{3}	2.2×10^{6}
7.2×10^{-2}	5.7×10^{1}	4.2×10^{-2}	1.4×10^{3}	2.1×10^{6}
7.8×10^{-2}	5.8×10^{1}	4.2×10^{-2}	1.4×10^{3}	2.2×10^{6}
8.5×10^{-2}	5.8×10^{1}	4.2×10^{-2}	1.4×10^{3}	2.1×10^{6}

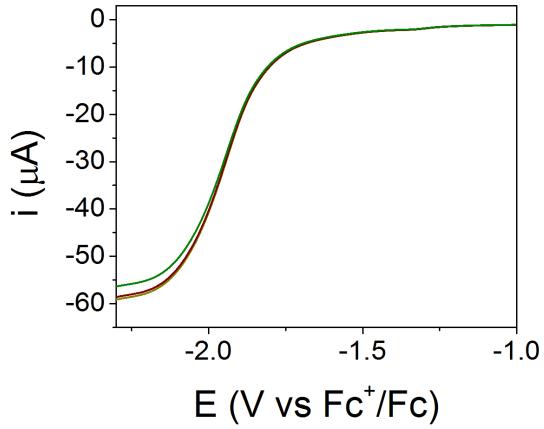

Figure S20. Voltammograms of 0.01 mM **Cu_2FP** recorded in a 0.1 M $TBAPF_6$ dichloromethane solution at a scan rate of 600 mV s^{-1} with 65 mM TFA using either a 3 mm glassy carbon disk (yellow) or a platinum wire (maroon and green) as the counter electrode. All voltammograms were recorded using a 1 mm diameter glassy carbon working electrode at room temperature and the ferrocenium/ferrocene redox couple as an internal reference. In these experiments, voltammograms were collected using the glassy carbon counter electrode prior to using the platinum counter electrode.

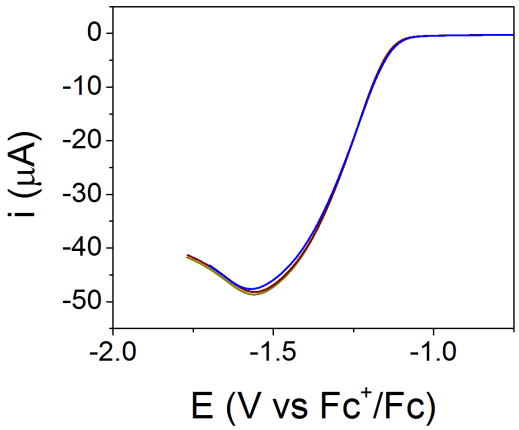

Figure S21. Voltammograms of 0.1 mM **Cu_2FP** recorded in a 0.1 M $TBAPF_6$ dichloromethane solution at a scan rate of 600 mV s^{-1} with 65 mM TFA using either a 3 mm glassy carbon disk (yellow) or a platinum wire (maroon and blue) as the counter electrode. All voltammograms were recorded using a 1 mm diameter glassy carbon working electrode at room temperature and the ferrocenium/ferrocene redox couple as an internal reference. In these experiments, voltammograms were collected using the glassy carbon counter electrode prior to using the platinum counter electrode.

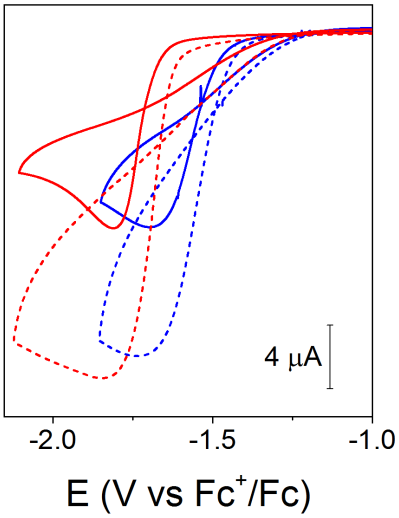

Figure S22. Cyclic voltammograms of 0.01 mM **Cu_2FP** (blue) and 0.01 mM **CuP** (red) recorded in a 0.1 M $TBAPF_6$ dichloromethane solution at a scan rate of 100 mV s^{-1} with either 16.25 mM (solid) or 32.5 mM (dashed) TFA. All voltammograms were recorded using a 1 mm diameter glassy carbon working electrode at room temperature and the ferrocenium/ferrocene redox couple as an internal reference. These are the cyclic voltammograms associated with the voltammetry data shown in Figure 5a of the main text.

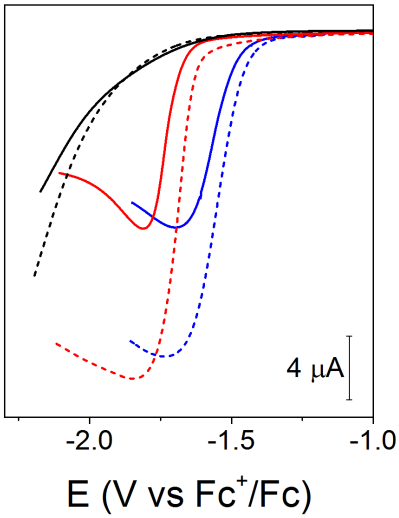

Figure S23. Voltammograms of 0.01 mM **Cu_2FP** (blue) and 0.01 mM **CuP** (red) recorded in a 0.1 M $TBAPF_6$ dichloromethane solution at a scan rate of 100 mV s^{-1} with either 16.25 mM (solid) or 32.5 mM (dashed) TFA. Voltammograms recorded using porphyrin-free solutions of 0.1 M $TBAPF_6$ in dichloromethane at a scan rate of 100 mV s^{-1} (black), with either 16.25 mM (solid) or 32.5 mM (dashed) TFA, are included for comparison. All voltammograms were recorded using a 1 mm diameter glassy carbon working electrode at room temperature and the ferrocenium/ferrocene redox couple as an internal reference.

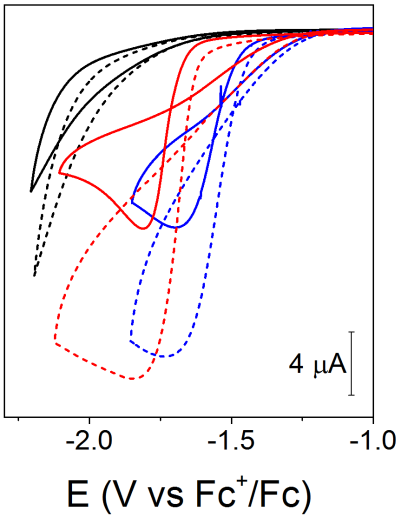

Figure S24. Cyclic voltammograms of 0.01 mM **Cu_2FP** (blue), and 0.01 mM **CuP** (red), recorded in a 0.1 M $TBAPF_6$ dichloromethane solution at a scan rate of 100 mV s^{-1} with either 16.25 mM (solid) or 32.5 mM (dashed) TFA. Voltammograms recorded using porphyrin-free solutions of 0.1 M $TBAPF_6$ in dichloromethane at a scan rate of 100 mV s^{-1} (black), with either 16.25 mM (solid) or 32.5 mM (dashed) TFA, are included for comparison. All voltammograms were recorded using a 1 mm diameter glassy carbon working electrode at room temperature and the ferrocenium/ferrocene redox couple as an internal reference.

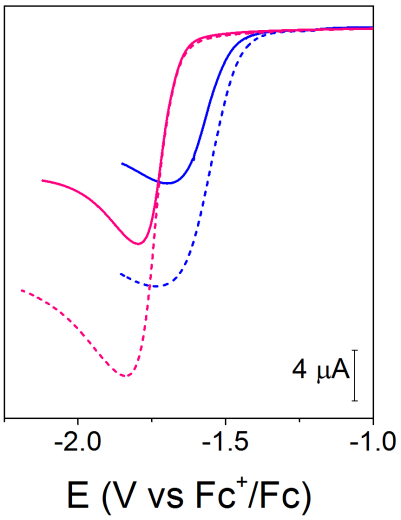

Figure S25. Voltammograms of 0.01 mM **Cu_2FP** (blue) and 0.02 mM **CuP** (pink) recorded in a 0.1 M $TBAPF_6$ dichloromethane solution at a scan rate of 100 mV s^{-1} with either 16.25 mM (solid) or 32.5 mM (dashed) TFA. All voltammograms were recorded using a 1 mm diameter glassy carbon working electrode at room temperature and the ferrocenium/ferrocene redox couple as an internal reference.

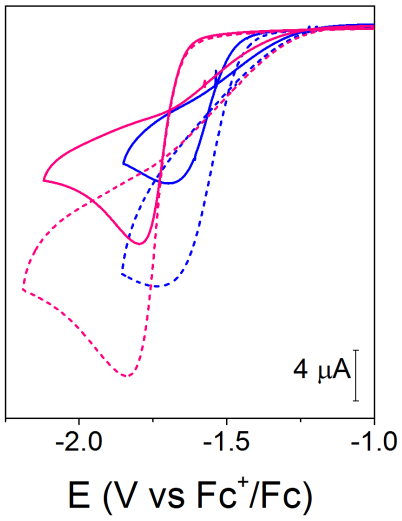

Figure S26. Cyclic voltammograms of 0.01 mM **Cu_2FP** (blue) and 0.02 mM **CuP** (pink) recorded in a 0.1 M $TBAPF_6$ dichloromethane solution at a scan rate of 100 mV s^{-1} with either 16.25 mM (solid) or 32.5 mM (dashed) TFA. All voltammograms were recorded using a 1 mm diameter glassy carbon working electrode at room temperature and the ferrocenium/ferrocene redox couple as an internal reference.

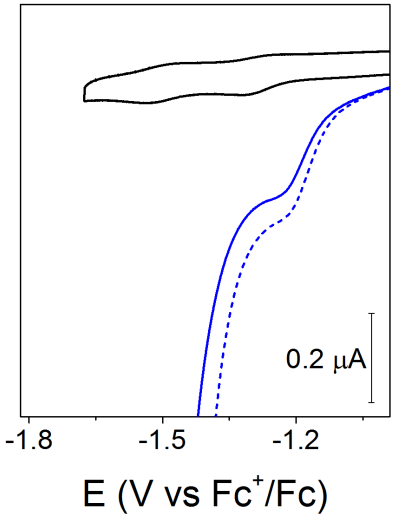

Figure S27. Voltammograms of 0.01 mM **Cu_2FP** recorded in a 0.1 M $TBAPF_6$ dichloromethane solution at a scan rate of 100 mV s^{-1} with either 0 mM (black solid), 16.25 mM (blue solid), or 32.5 mM (blue dashed) mM TFA. All voltammograms were recorded using a 1 mm diameter glassy carbon working electrode at room temperature and the ferrocenium/ferrocene redox couple as an internal reference.

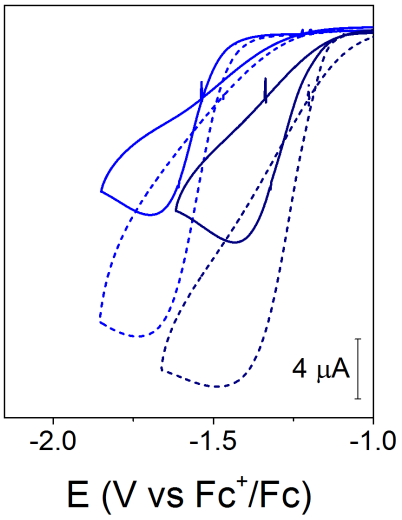

Figure S28. Cyclic voltammograms of 0.01 (blue) and 0.1 (dark blue) mM **Cu_2FP** recorded in a 0.1 M $TBAPF_6$ dichloromethane solution at a scan rate of 100 mV s^{-1} with either 16.25 mM (solid) or 32.5 mM (dashed) TFA. All voltammograms were recorded using a 1 mm diameter glassy carbon working electrode at room temperature and the ferrocenium/ferrocene redox couple as an internal reference. These are the cyclic voltammograms associated with the voltammetry data shown in Figure 5b of the main text.

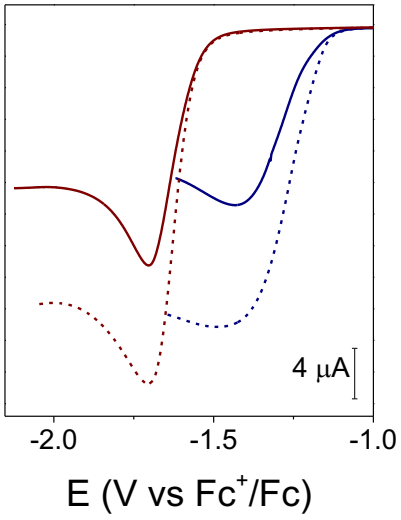

Figure S29. Voltammograms of 0.1 mM **Cu_2FP** (dark blue) and 0.1 mM **CuP** (dark red) recorded in a 0.1 M $TBAPF_6$ dichloromethane solution at a scan rate of 100 mV s^{-1} with either 16.25 mM (solid) or 32.5 mM (dashed) TFA. All voltammograms were recorded using a 1 mm diameter glassy carbon working electrode at room temperature and the ferrocenium/ferrocene redox couple as an internal reference.

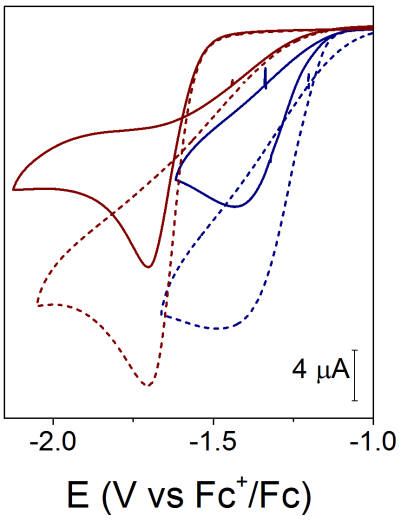

Figure S30. Cyclic voltammograms of 0.1 mM **Cu_2FP** (dark blue) and 0.1 mM **CuP** (dark red) recorded in a 0.1 M $TBAPF_6$ dichloromethane solution at a scan rate of 100 mV s^{-1} with either 16.25 mM (solid) or 32.5 mM (dashed) TFA. All voltammograms were recorded using a 1 mm diameter glassy carbon working electrode at room temperature and the ferrocenium/ferrocene redox couple as an internal reference.

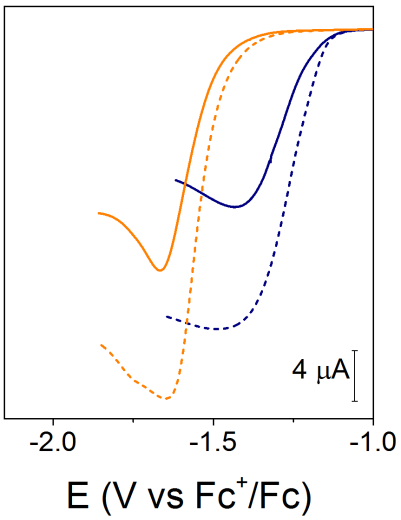

Figure S31. Voltammograms of 0.1 mM **Cu_2FP** (dark blue) and 0.2 mM **CuP** (orange) recorded in a 0.1 M $TBAPF_6$ dichloromethane solution at a scan rate of 100 mV s^{-1} with either 16.25 mM (solid) or 32.5 mM (dashed) TFA. All voltammograms were recorded using a 1 mm diameter glassy carbon working electrode at room temperature and the ferrocenium/ferrocene redox couple as an internal reference.

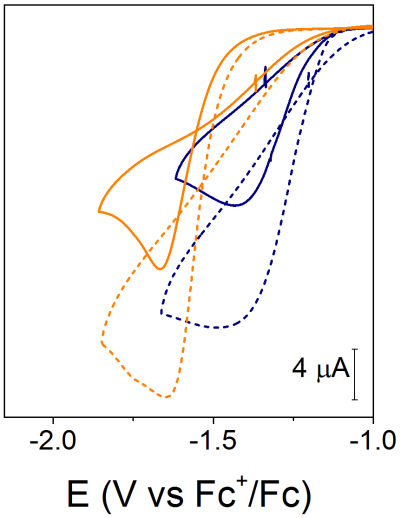

Figure S32. Cyclic voltammograms of 0.1 mM **Cu_2FP** (dark blue) and 0.2 mM **CuP** (orange) recorded in a 0.1 M $TBAPF_6$ dichloromethane solution at a scan rate of 100 mV s^{-1} with either 16.25 mM (solid) or 32.5 mM (dashed) TFA. All voltammograms were recorded using a 1 mm diameter glassy carbon working electrode at room temperature and the ferrocenium/ferrocene redox couple as an internal reference.

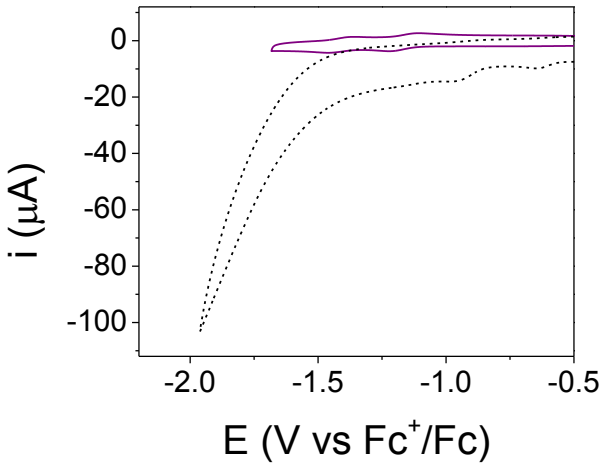

Figure S33. Cyclic voltammograms of *meso*-β doubly-fused 5,24-di(*p*-tolyl)-10,19,29,38-tetramesityl porphyrin (0.1 mM) recorded in a 0.1 M $TBAPF_6$ dichloromethane solution at a scan rate of 500 mV s^{-1} with either 0 mM (purple) or 6.5 mM (black) TFA. All voltammograms were recorded using a 3 mm diameter glassy carbon working electrode at room temperature and the ferrocenium/ferrocene redox couple as an internal reference.

8. Rotating Ring-Disk Experiments

Figure S34. Photograph of the electrochemical setup used for rotating ring-disk experiments.

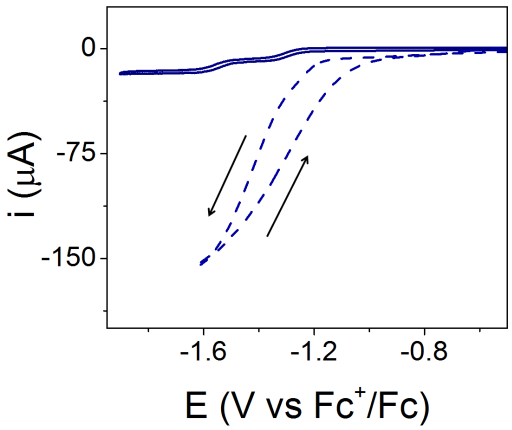

Figure S35. Cyclic voltammograms of 0.1 mM **Cu_2FP** (dark blue) recorded in a 0.1 M $TBAPF_6$ dichloromethane solution with 0 mM (solid) and 2.6 mM (dash) TFA at a scan rate of 100 mV s^{-1}. All voltammograms were recorded using a 5 mm diameter glassy carbon working electrode rotating at 1000 RPM at room temperature and the ferrocenium/ferrocene redox couple as an internal reference.

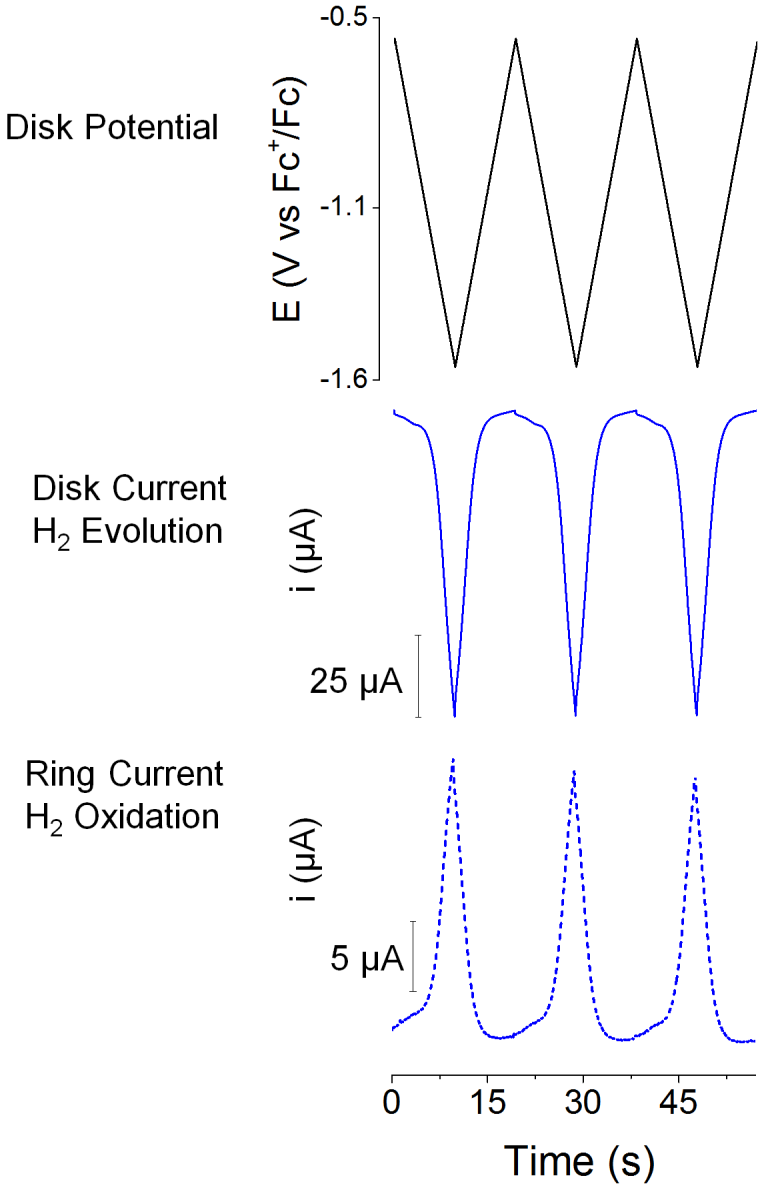

Figure S36. Rotating ring-disk measurements (100 mV s^{-1}) of hydrogen evolution using 0.1 mM **Cu_2FP** in a dichloromethane solution with 0.1 M $TBAPF_6$ electrolyte and 2.6 mM TFA at a glassy carbon electrode. (Top) GC disk potential. (Middle) GC disk current. (Bottom) Pt-ring current (the Pt ring was held at 0.79 V vs Fc^+/Fc).

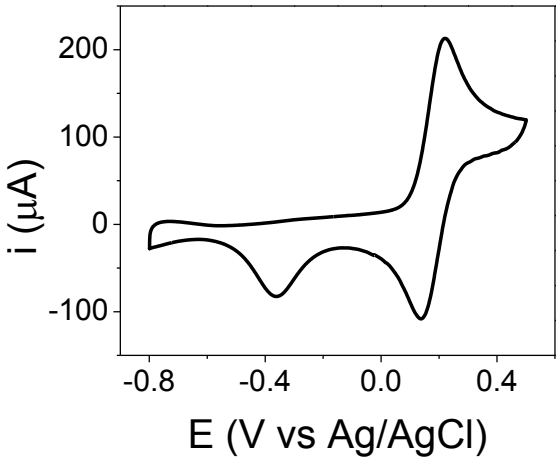

Figure S37. Cyclic voltammogram of 10 mM $K_4Fe^{II}(CN)_6$ recorded in a 0.1 M NaOH aqueous solution at a scan rate of 100 mV s^{-1} using the platinum ring of the rotating ring-disk setup as a working electrode.

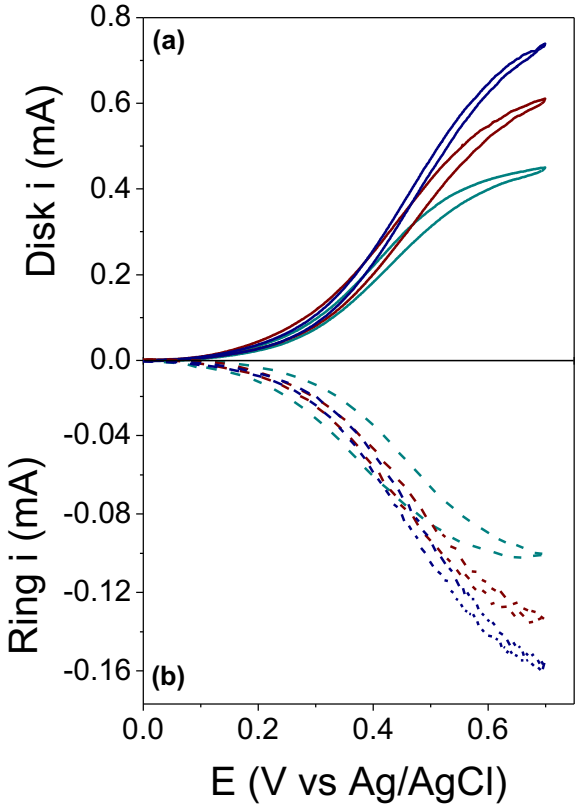

Figure S38. (a) Cyclic voltammograms of 10 mM $K_4Fe^{II}(CN)_6$ recorded in a 0.1 M NaOH aqueous solution at a scan rate of 100 mV s^{-1} using a 5 mm diameter glassy carbon working electrode disk rotating at 500 (cyan), 1000 (dark red), and 1500 (dark blue) RPM. (b) Current response of the platinum ring when polarized at -0.1 V vs Ag/AgCl for each of the rotating conditions. The x-axis values indicate the applied potential at the glassy carbon disk electrode.

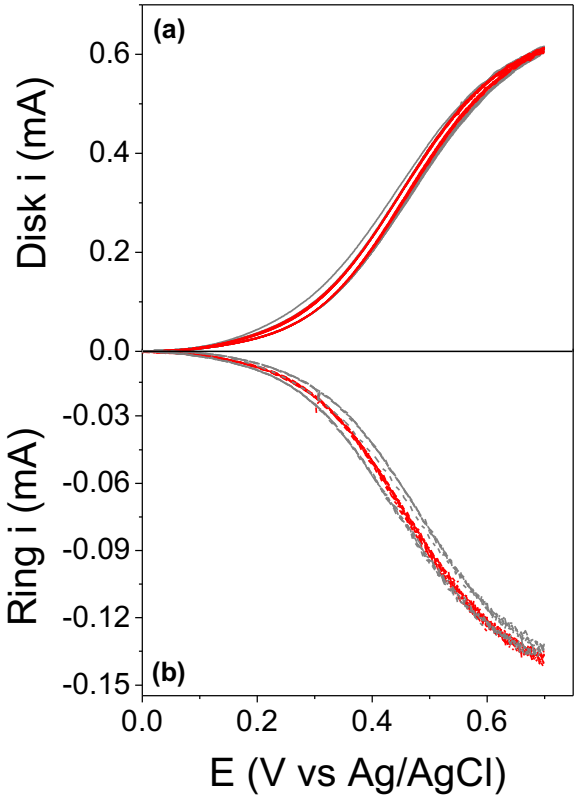

Figure S39. (a) Cyclic voltammograms of 10 mM $K_4Fe^{II}(CN)_6$ recorded in a 0.1 M NaOH aqueous solution at scan rates of 25 mV s^{-1} (red) and 100 mV s^{-1} (gray) using a 5 mm diameter glassy carbon working electrode disk rotating at 1000 RPM. (b) Current response of the platinum ring when polarized at -0.1 V vs Ag/AgCl for different scan conditions at the disk. The x-axis values indicate the applied potential at the glassy carbon disk electrode.

9. Acid Stability

UV–vis-NIR spectra and mass spectrometry data were collected following exposure of **Cu_2FP** to a concentration of TFA required to access the S-shaped waves described in this report (7000-fold excess in acid) and show no evidence of the demetallated **Cu_2FP** species. However, these results do indicate the presence of absorption bands associated with the chemically oxidized form of **Cu_2FP** that is present at these relatively high concentrations of acid, consistent with absorption spectra of **Cu_2FP** collected during thin-layer constant potential electrolysis generating **Cu_2FP^{1+}** (Figure S9c).

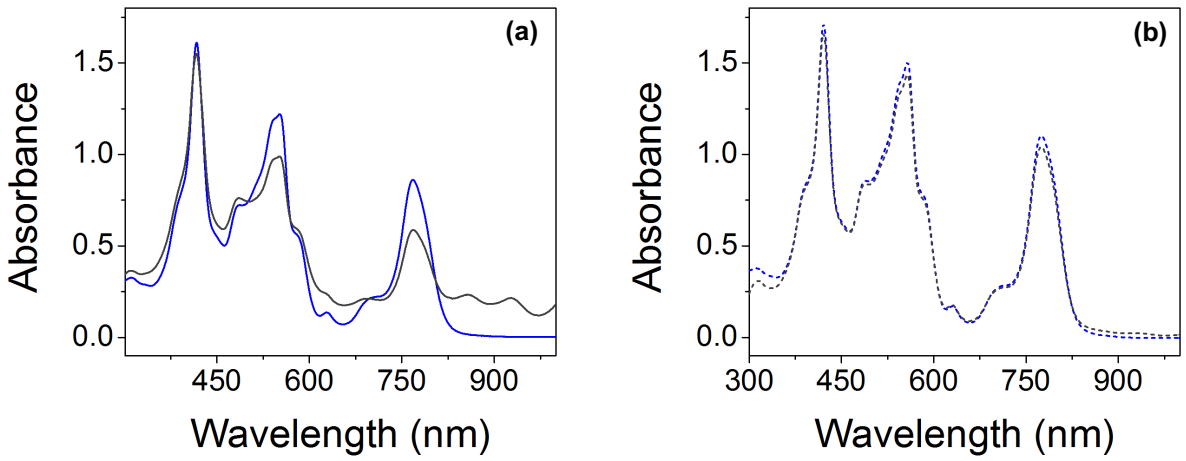

Figure S40. Absorption spectra of **Cu_2FP** (12.5 μM) recorded in (a) dichloromethane or (b) benzonitrile in the absence (blue) or presence (black) of TFA (87.5 mM) after 4 hours.

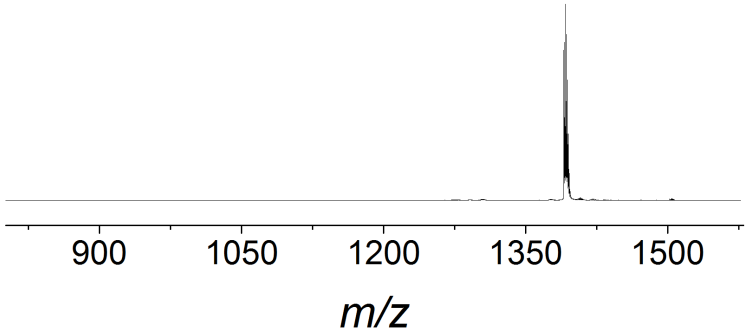

Figure S41. MALDI-TOF MS data collected using samples of **Cu_2FP** following 4 hours of exposure to a solution of 87.5 mM TFA (7000 equivalents of TFA with respect to the concentration of **Cu_2FP** used in these experiments / 12.5 μM in **Cu_2FP**) in dichloromethane. The isotopic distribution pattern is consistent with that collected for a pure sample **Cu_2FP** (1390.45 *m*/*z*), showing no detectable presence of demetallated free-base fused porphyrin (1268.62 *m*/*z*) or other decomposition products.

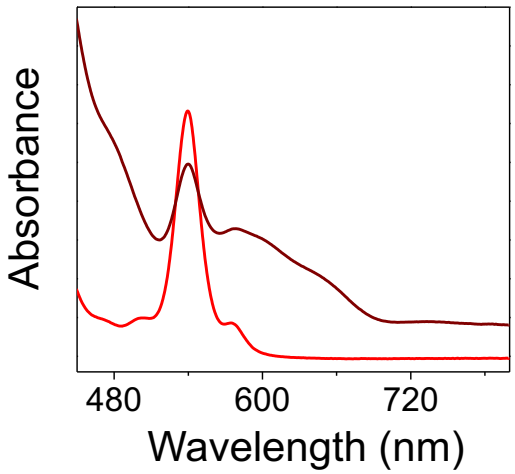

Figure S42. Absorption spectra of **CuP** (15 μM) recorded in dichloromethane in the absence (red) or presence (dark red) of TFA (mM 106) after 4 hours.

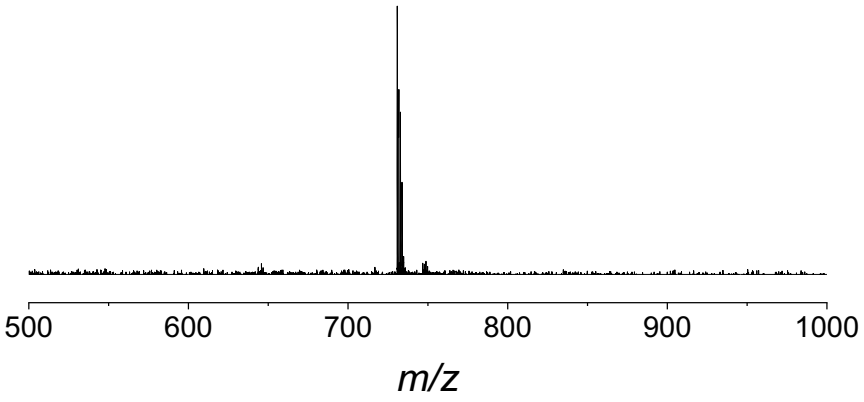

Figure S43. MALDI-TOF MS data collected using samples of **CuP** following 4 hours of exposure to a solution of 106 mM TFA (7000 equivalents of TFA with respect to the concentration of **CuP** used in these experiments / 15 μM in **CuP**) in dichloromethane. The isotopic distribution pattern is consistent with that collected for a pure sample **CuP** (731.22 *m*/*z*), showing no detectable presence of demetallated free-base porphyrin (670.31 *m*/*z*) or other decomposition products.

10. The HA/H_2 Equilibrium Potential in Dichloromethane

All measurements were conducted following a previously reported procedure and experimental setup.[7]

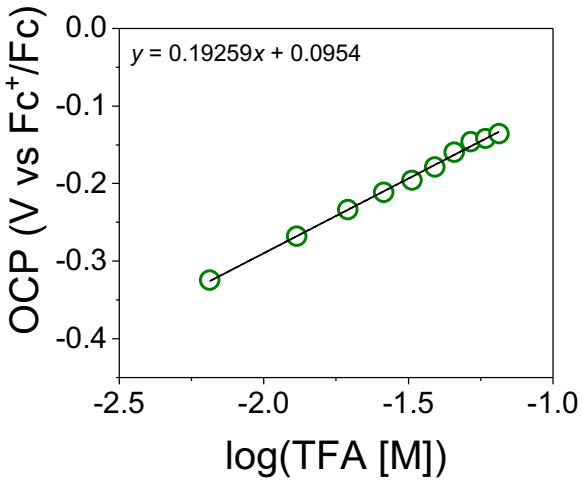

Figure S44. Open circuit potential (OCP) of a hydrogen-flame treated platinum electrode versus Fc^+/Fc as a function of log([TFA]) in a 0.1 M $TBAPF_6$ dichloromethane solution collected under 1.0 atm hydrogen. OCP (V vs Fc^+/Fc) = 0.19259 log([TFA]) + 0.0954. R^2 = 0.997.

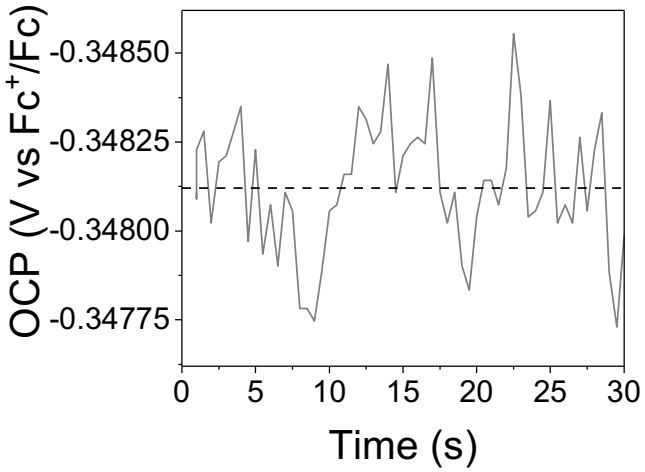

Figure S45. OCP of a hydrogen-flame treated platinum electrode versus Fc^+/Fc as a function of time. This data was collected in a 0.1 M $TBAPF_6$ dichloromethane solution and represents one data point used to determine E_{HA}/E_{H_2} for a particular solution composition.

11. Supporting Information References

(1) Hariprasad, G.; Dahal, S.; Maiya, B. G. meso-Substituted Octabromoporphyrins: Synthesis, Spectroscopy, Electrochemistry and Electronic Structure. *J. Chem. Soc., Dalton Trans.* **1996**, *16*, 3429–3436.

(2) Gervaldo, M.; Fungo, F.; Durantini, E. N.; Silber, J. J.; Sereno, L.; Otero, L. Carboxyphenyl Metalloporphyrins as Photosensitizers of Semiconductor Film Electrodes. A study of the Effect of Different Central Metals. *J. Phys. Chem. B* **2005**, *109*, 20953–20962.

(3) Ye, L.; Ou, Z.; Fang, Y.; Xue, S.; Song, Y.; Wang, L.; Wang, M; and Kadish, K. M. Electrochemistry of Nonplanar Copper (II) Tetrabutano- and Tetrabenzotetraarylporphyrins in Nonaqueous Media. *RSC Adv*. **2015**, *5*, 77088–77096.

(4) Brennan, B. J.; Arero, J.; Liddell, P. A.; Moore, T. A.; Moore, A. L.; Gust, D. Selective Oxidative Synthesis of Meso-beta Fused Porphyrin Dimers. *J. Porphyrins Phthalocyanines* **2013**, *17*, 247–251.

(5) Weil, J. A.; Bolton, J. R. *Electron Paramagnetic Resonance: Elementary Theory and Practical Applications*. John Wiley & Sons. **2007**.

(6) Stoll, S.; Schweiger, A. J. EasySpin, a Comprehensive Software Package for Spectral Simulation and Analysis in EPR. *Magn. Reson.* **2006**, *178*, 42–55.

(7) Roberts, J. A.; Bullock, R. M. Direct Determination of Equilibrium Potentials for Hydrogen Oxidation/Production by Open Circuit Potential Measurements in Acetonitrile. *Inorg. Chem.* **2013**, *52*, 3823–3835.